

Gradient-based Automatic Mixed Precision Quantization for Neural Networks On-Chip

Chang Sun,^{1,2,*} Thea K. Årrestad,¹ Vladimir Loncar,^{3,4} Jennifer Ngadiuba,⁵ and Maria Spiropulu²

¹*ETH Zurich (Zurich, Switzerland)*

²*California Institute of Technology (CA, USA)*

³*Massachusetts Institute of Technology (MA, USA)*

⁴*Institute of Physics Belgrade (Belgrade, Serbia)*

⁵*Fermi National Accelerator Laboratory (IL, USA)*

Model size and inference speed at deployment time, are major challenges in many deep learning applications. A promising strategy to overcome these challenges is quantization. However, a straightforward uniform quantization to very low precision can result in significant accuracy loss. Mixed-precision quantization, based on the idea that certain parts of the network can accommodate lower precision without compromising performance compared to other parts, offers a potential solution. In this work, we present High Granularity Quantization (HGQ), an innovative quantization-aware training method that could fine-tune the per-weight and per-activation precision by making them optimizable through gradient descent. This approach enables ultra-low latency and low power neural networks on hardware capable of performing arithmetic operations with an arbitrary number of bits, such as FPGAs and ASICs. We demonstrate that HGQ can outperform existing methods by a substantial margin, achieving resource reduction by up to a factor of 20 and latency improvement by a factor of 5 while preserving accuracy.

I. INTRODUCTION

Edge computing has significantly increased the importance of real-time deep neural network inference on specialized hardware [1]. While the typical latency threshold for real-time inference applications is $\mathcal{O}(1)$ ms [2–4], certain domains require sub-microsecond inference times. At the CERN Large Hadron Collider (LHC) [5], detectors generate hundreds of terabytes of data every second from proton-proton collisions occurring every 25 nanoseconds. This enormous data throughput is reduced by the *trigger*, a hardware system filtering data in real-time at the same rate. This detector subsystem determines the fate of each collision event – whether it should be preserved for offline processing or discarded – with a decision-making latency ceiling at a few microseconds [6, 7]. The trigger’s accuracy is vital to retain only the interesting events for physics studies, thereby managing the downstream bandwidth effectively by reducing the data rate by two orders of magnitude. The system consists of $\mathcal{O}(1000)$ field programmable gate arrays (FPGAs), where several algorithms are running in parallel on each FPGA. As a result, resources are scarce and the spacial complexity of each algorithm needs to be minimal. In anticipation of the LHC’s upgrade to the High Luminosity-LHC (HL-LHC) [8], which will increase data rates and complexity by a factor of 1-2, machine learning techniques are being actively explored to enhance the speed and accuracy of the algorithms in the future trigger

system [6, 7]. However, integrating demanding models under such strict resource and latency constraints without compromising performance is a hurdle. To satisfy the latency requirements, neural networks on FPGAs for LHC physics experiments are usually fully unrolled – all arithmetic operations are done by different components in the circuit without overlapping – and pipelined to minimize the latency and maximize the throughput at the cost of higher resource consumption. Efforts in recent years have focused on algorithmic efficiency, with strategies ranging from the design of compact networks to weight pruning and quantization [9, 10].

Quantization is a model compression technique that converts model parameters into lower-precision formats, resulting in some performance degradation in exchange for a smaller model size and/or faster inference. To quantize a neural network, one can either reduce the precision of its parameters after training or train the network directly with low precision parameters. These two approaches are referred to as post-training quantization (PTQ) and quantization-aware training (QAT), respectively. While PTQ is computationally cheaper to perform in general, it usually induces a more significant loss in performance compared to QAT under the same compression ratio. To aim for the best possible trade-off between model performance and resource consumption, we follow the QAT approach.

In this work, we introduce high-granularity quantization (HGQ), a novel QAT method that optimizes the quantization bitwidths during training using gradients, which enables models to be quantized at arbitrary granularity. In contrast to existing methods, where

* E-mail: chsun@cern.ch

bitwidths for network parameters are optimized in pre-defined, structured blocks, HGQ provides more granular control over which parameters share the same bitwidth. For models deployed with fully unrolled implementations like the ones used in the trigger systems, every parameter in the network may have its unique bitwidth. We illustrate the key difference between the HGQ method and the conventional block-wise quantization methods in Figure I. Optimizing the bitwidths at higher granularity allows HGQ to find better trade-offs between the model performance and resource consumption. Furthermore, by optimizing these individual bitwidths alongside the network using gradient descent, the need for including the bitwidths as hyperparameters to be optimized with iterative trainings is eliminated. Depending on the specific task, we demonstrate that HGQ has the potential to outperform other model compression methods and achieve resource reduction by up to a factor of 20, and latency improvement by a factor of 5 while preserving the model performance.

A functional HGQ library has been developed with `Tensorflow` [11] and `Keras` [12], and we have released it as a free and open-source software. The Vivado/Vitis® FPGA back-ends are supported through integration with `hls4ml` [13] – a software tool designed to facilitate the conversion of machine learning algorithms into hardware designs, which is specifically optimized for ultra-low latency deployment on FPGAs and application-specific integrated circuits (ASICs)[14] through High-Level Synthesis (HLS). The HGQ library guarantees an exact correspondence between the software and firmware models, provided that no numeric overflow occurs and intermediate values are exactly representable by the floating-point datatype used in emulation.

The work presented here makes the following contributions:

- We present a new algorithm for obtaining surrogate gradients for the quantization bitwidths, derived from both the loss function and the estimated model resource consumption, enabling full gradient-based optimization of bitwidths;
- We propose a new metric named Effective Bit Operations (EBOPs) for accurate estimation of a model’s on-chip resource consumption;
- We enable heterogeneous quantization of a specific model at arbitrary granularity up to per-parameter level, aiming to minimize hardware resource usage while preserving the performance. This approach automatically includes sparse pruning of the network parameters as their bitwidths reach zero;
- We have made the HGQ library easily accessible online[15], and user-friendly: A simple drop-in replacement of the `Keras` layers makes it straightforward for users to transform `Keras` models to their corresponding heterogeneously quantized versions;
- We have added support for HGQ-trained models in the `hls4ml` tool, which converts these pre-trained quantized models into highly-parallel

FPGA firmware with HLS. We ensure bit-level consistency between the software model and the corresponding firmware, making the library safe and easy to use for non-experts;

- compared to other state-of-the-art model compression methods targeting ultra-low latency applications, we demonstrate a resource reduction of up to 95% and an improvement in latency of up to 5-fold by using HGQ, all while maintaining accuracy.

II. RELATED WORK

Quantization is a widely adopted method for compressing deep neural networks (DNNs) for implementing them on specialized hardware devices such as FPGAs or ASICs. Previous studies have utilized extremely low precision quantization, such as binary or ternary, across networks to enhance throughput and reduce latency. Binary quantization restricts parameters to $\alpha \times \{-1, 1\}$ (or $\alpha \times \{0, 1\}$ in some convention), and ternary to $\alpha \times \{-1, 0, 1\}$, with α being a relatively high-precision scaling factor. Key examples include DoReFa Net [16], ABC-net [17], Binaryconnect [18], XNOR-net [19], TWN [20], TTQ [21], and [22]. While these methods could achieve high model compression ratios, they come at the cost of substantially reduced model performance compared to the corresponding float-point baselines. Using the same principles as binary networks, several studies have moved to multi-bit network designs that represent weights through binary bases and values, highlighted in works like [17, 23–27].

Many studies have investigated heterogeneous quantization with layer/channel-specific precision to lessen the performance loss due to quantization. In particular, HAQ [28] and AutoQ [29] utilize reinforcement learning to find optimal bitwidth configurations. HAWQ, HAWQ-V2, PyHessian, Q-BERT, and OBQ [30–34] focus on optimizing bitwidths with the second-order approximations of the loss function around the unquantized optimal weights. DNAS [35] and AutoQKeras [36] optimize the bitwidths and network architecture simultaneously. IN particular, DNAS uses stochastic sampling to obtain a subnetwork from a super network, and AutoQKeras employs gradient-free methods like Gaussian Process, Hyperband, and stochastic search for hyperparameter optimizations. Similarly, Meta-ML [37] applies iterative optimizations to various hyperparameters, including the bitwidths, weight pruning strategy, and model architecture. FILM-QNN [38] optimizes weight and activation’s bitwidths in a manner conducive to hardware efficiency for convolutional neural networks. For each convolutional layer, it categorizes filters into two groups of lower and higher precision based on the anticipated loss of performance due to quantizing each filter, and arranges them to utilize the on-board multipliers on FPGAs efficiently.

Heterogeneous quantization at sub-layer/channel granularity is also studied by other works. RVQuant [39],

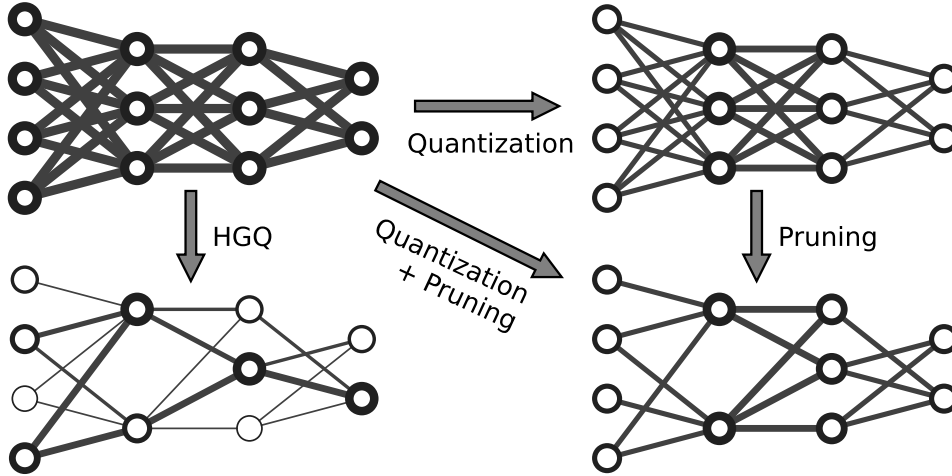


FIG. I. An illustration of the HGQ method on a dense network. Activation and weights of the network are shown in circles and lines, with the thickness indicating the corresponding bitwidth. A line/circle is dropped when the corresponding value is pruned. Top left: baseline network with high precision throughout. Top right: a layer-wise heterogeneously quantized network, e.g., trained with QKeras. Bottom right: a network that is both layer-wise heterogeneously quantized and unstructured pruned. Bottom left: a network trained with HGQ with maximum granularity: Each weight and activation has its unique bitwidth. When a bitwidth reaches zero, the corresponding values is effectively pruned.

BitsandBytes [40], SpQR [41], and SqueezeLLM[42] offloads a small fraction of outlier weights to higher precision formats to mitigate the performance degradation due to quantization. These works primarily targets for the weight size reduction of larger models, rather than efficient inference on specialized hardware like FPGAs or ASICs.

Pruning is another technique used to compress neural networks. It involves the removal of weights in a network that have minimal impact on the overall performance. This concept was first introduced in [43], and first applied to neural networks in [44]. The removal of weights is sometimes formulated by pruning masks – binary valued tensors that are multiplied with the weights to zero out the pruned ones.

Depending on how the pruned weights are arranged, pruning can be categorized as structured or unstructured pruning. Structured pruning removes weights in specific blocks or following certain patterns, usually in a hardware-friendly manner to speed up the inference, as in [45–50]. On the other hand, unstructured pruning targets individual weights for the best compression ratio, as in [51–55]. Semi-structured pruning targeting specific hardware accelerators also exists, as in [50, 56].

On methodology side, [34, 44, 48, 50] use Hessian of the loss function for determining the optimal pruning mask and weight compensations post-training. [47] formulates the pruning mask creation as an optimal transport problem and then relaxes it to be differentiable for training. [49, 55] directly use trainable pruning masks that are optimized along with the weights. [52, 53] remove weights with the small magnitude iteratively during training. [54] optimizes the pruning mask by solving it as a constraint

optimization problem during training with the stochastic Frank-Wolfe algorithm. With a similar objective to this work, [45] solves the post-training pruning problem with constraint programming to reduce the network’s on-chip resource usage.

In this work, we consider pruning as a special form of quantization, where the pruned weights are quantized with zero bits. In this way, pruning is automatically done by optimizing the quantization bitwidths during training.

Closely related to this work, the QKeras [36] framework aims to train and optimize neural networks for deployment on FPGAs and ASICs. QKeras is developed on top of Keras and leverages hls4ml [57] for hardware deployment. It enables training and optimization of neural networks with hardware-friendly fixed-point numbers for both weights and activations. AutoQKeras, a feature within QKeras, enables automatic adjustment of quantization settings for each layer using gradient-free approaches.

Brevitas [58] serves as the PyTorch [59] equivalent of QKeras, which is commonly used in pair with the FINN and FINN-R frameworks from Xilinx Research [60, 61] for deploying on AMD[®] FPGAs.

III. HIGH GRANULARITY QUANTIZATION

In this work, we introduce High Granularity Quantization (HGQ), a novel quantization approach with the unique capability of optimizing the bitwidths in a quantized neural network at arbitrary fine granularity – up to per-parameter level. At the same time, it provides an accurate on-chip resource usage estimation, and simulta-

neously optimizes the accuracy and resource usage of the network in a hardware/software co-design fashion. We begin this section by outlining the fundamentals of quantization and quantization-aware training. Then, we introduce a way to accurately estimate the on-chip resource consumption of a model. Subsequently, we introduce an innovative gradient-based technique for auto-tuning the bitwidths during training. A comprehensive explanation of the HGQ method and its algorithm follows.

A. Quantization

Quantization is a map, henceforth referred to as f^q , from the set of real numbers \mathbb{R} to a discrete subset $\mathbb{Q} \equiv \{q_i | q_{i+1} > q_i\} \subset \mathbb{R}$. For hardware efficiency, we ensure that quantized weights and activations are represented as fixed-point numbers, a common practice in hardware for numerical representation. A fixed-point number can be understood as an integer scaled by a factor of powers of two. It is characterized by its bitwidth (total number of bits) and the number of bits allocated for the integer part. The inclusion of the sign bit in the integer part for signed numbers varies by convention. In this context, we adhere to the convention used in AMD[®] Vivado/Vitis[®] HLS, which includes the sign bit in the integer part if presents. We denote the bitwidth $b \in \mathbb{N}_+$ with $i \in \mathbb{Z}$ bits are dedicated to the integer part, and define $f \equiv b - i$ as the number of fractional bits. For a signed fixed-point number, its representable range is $[-2^{i-1}, 2^{i-1} - 2^{-f}]$ with a step size of 2^{-f} . For an unsigned fixed-point number, the range is $[0, 2^i - 2^{-f}]$ with the same step size.

One way of quantizing a real number into a signed fixed-point number, `fixed<b,i>`, can be expressed as

$$\begin{aligned} f^q(x) &= (([x \cdot 2^f] + 2^{b-1} \bmod 2^b) - 2^{b-1}) \cdot 2^{-f} \\ &= \begin{cases} [x \cdot 2^f] \cdot 2^{-f}, & \text{if } x \in [-2^{i-1}, 2^{i-1} - 2^{-f}] \\ \text{overflow} & \text{otherwise} \end{cases}, \end{aligned} \quad (1)$$

where $[x] \equiv [x + \epsilon]$ with some $\epsilon \in [0, 1)$ and $f \equiv b - i$. Note that setting $\epsilon = 1/2$ recovers conventional round to the nearest neighbor rounding with midpoint round-up. Similarly to the signed case, for an unsigned fixed-point number denoted as `ufixed<b,i>`, a quantization procedure can be expressed as

$$\begin{aligned} f^q(x) &= ([x \cdot 2^f] \bmod 2^b) \cdot 2^{-f} \\ &= \begin{cases} [x \cdot 2^f] \cdot 2^{-f}, & \text{if } x \in [0, 2^i - 2^{-f}] \\ \text{overflow} & \text{otherwise} \end{cases}. \end{aligned} \quad (2)$$

In Eq. (1) and (2), ‘‘overflow’’ refers to that the value to be quantized exceeds the representable range of the fixed-point number, which then cause a cyclical wrap of the number to the opposite end of the range. Although a quantization function could be designed to adjust values outside the permissible range to the closest valid

value (i.e., clipping them into the range), this approach is avoided in our work to reduce resource and latency overhead. Instead, by selecting an optimal set of quantization parameters, we ensure that the all numbers produced during inference falls into the representable range to avoid overflow.

In our approach, we track only the number of fractional bits f of the fixed-point numbers during training for quantization. Before deploying to hardware, we estimate the required number of integer bits i to avoid overflow. This task is trivial for weights, as their values are fixed after training. For intermediate accumulator and activation values, we employ a calibration dataset to gauge the extremes (both maximum and minimum) the values might assume. This process involves running the dataset through the network and logging the extreme quantized values (v_{\min}^q, v_{\max}^q), from which we can determine the necessary integer bitwidth without the sign bit i' using

$$i' = \max(\lfloor \log_2 |v_{\max}^q| \rfloor + 1, \lceil \log_2 |v_{\min}^q| \rceil) \quad (3)$$

and obtain the integer bitwidth i by add back the sign bit when necessary: $i = i' + 1$ for signed fixed-point numbers, and $i = i'$ for unsigned fixed-point numbers.

By ensuring the calibration dataset accurately reflects the input data distribution the network will encounter after deployment, we can avoid the overflows in inference time. For extra safety, one may add extra margins to the computed ranges to account for potential outliers in the input data. This method thus eliminates the need to consider the representable ranges of the given quantizer during the training phase, and the quantization function during training can now be expressed as:

$$f^q(x) = [x \cdot 2^f] \cdot 2^{-f} = \lfloor (x + \epsilon) \cdot 2^f \rfloor \cdot 2^{-f}. \quad (4)$$

Without loss of generality, we assume $\epsilon = 1/2$ for the rest of this section and recover the conventional midpoint round-up rounding. This assumption will not affect any of the conclusions drawn in this work.

B. Quantization-Aware Training

Quantization-aware training (QAT) trains neural networks by applying quantization directly during the training phase. Previous works, e.g. [36], demonstrate that QAT significantly mitigates the performance degradation caused by post-training quantization. In this work, we adopt the same QAT scheme utilized in [36] for our HGQ method. Specifically, we employ the straight-through estimator (STE) [62] for quantization of weights and activations, which quantizes the values during the forward pass while acts as an identity for computing the gradients in the backward pass.

C. FPGA resource consumption estimation

A common metric for estimating on-chip resource usage in FPGAs is Bit Operations (BOPs) proposed in [63]. BOPs quantify the resource consumption by counting the number of bits involved in all operations performed during the network’s forward pass. For two numbers declared in bitwidths b_i and b_j , the number of BOPs is $b_i \cdot b_j$ for a multiplication operation, and the resultant number’s bitwidth for an addition operation. While BOPs could be a good resource indicator in many cases, it falls short in accurately reflecting resource consumption for unrolled neural networks on specialized hardware. The major discrepancies arise from the following two points:

1. Declaring a constant as a fixed-point format number of b bits does not necessarily mean that all b bits are used. For instance, a weight of 0.5 in an 8-bit fixed-point format only uses 1 bit instead of 8 bits, and counting it as 8 for BOPs computation leads to an inaccurate resource usage estimation.
2. BOPs tends to overestimate the resource consumption of accumulation operations compared to multiplications. Generally, most of the multiplication operations in neural networks are between a fixed constant and a variable as a part of vector-dot-products. Consider a single multiplication involving two numbers of each of b_i and b_j bits where the first number is a constant: When unrolled, this operation is often decomposed into an accumulation of $\sim (b_i - 1)$ shifted numbers each of b_j bits on hardware. By BOPs definition, this would be count as approximately $b_j \cdot (b_i - 1) + b_i^2$ operations in accumulation, which is much greater than $b_i \cdot b_j$ in general.

To address this discrepancy and offer a more precise estimation of on-chip resource usage, we propose a novel metric, Effective Bit Operations (EBOPs). For computing EBOPs, the bitwidth used for constants is not the declared bitwidth, but the number of bits enclosed by non-zero bits in binary form. For instance, a weight represented as 001xx1000 will be counted as 4 bits instead of 8 bits. This approach ensures that the resource consumption is not overestimated by the declared bitwidth. If multiple weights share the same multiplier (e.g., partially unrolling), the bitwidth of that weight group is defined by the number of bits enclosed by the most and least significant non-zero bits in that weight group. For simplicity, we consider only the absolute values of parameters when computing the bitwidths.

To address the second issue, we let the accumulation of N shifted numbers, each of b bits, to be count as $N \cdot b$ EBOPs. As a result, EBOPs contributed by a multiplication inside an accumulation chain (e.g., inside a vector dot product) is still the product of the operands’ bitwidths, as the accumulation operation of the resultant number is already implicitly counted.

Hence, EBOPs effectively count only the BOPs conducted during multiplicative processes in a network with the modified bitwidth definition. Let $\mathcal{M} = \{\{i, j\}_n\}$ be the set of all multiplication operations between operands with bitwidths b_i and b_j . The total number of EBOPs can then be expressed as

$$\text{EBOPs} = \sum_{i, j \in \mathcal{M}} b_i \cdot b_j. \quad (5)$$

Experimental findings validate EBOPs as a reliable estimator for on-chip resource consumption, which closely mirrors a linear combination of (look-up tables) LUT and digital signal processors (DSPs) usages. Detailed results are discussed in Section V. To get an accurate resource estimation from EBOPs, one should only include operations that will be executed in parallel. For instance, different inputs fed to the same multiplier through a buffer should be counted only once. Additionally, this estimation does not include overhead from non-multiplication-accumulation processes (e.g., buffers, logic switches, array indexing). For a complete resource usage estimation, one need to estimate them separately in other means and add these additional resource consumption to the EBOPs estimation.

D. Gradient-based optimization of bitwidths

To obtain a fully-unrolled quantized neural network with minimum usage on-chip, we want the ability to optimize the bitwidth of each individual weight and activations. However, as the number of bitwidths to be optimized would exceed the number of trainable parameters in the original network in this way, we propose the use of a gradient-based method to handle this vast parameter space. Nonetheless, direct optimization of these bitwidths via gradients is not possible due to their discreteness and the lack of gradients on them. Therefore, we address two main issues: *a)* make the discrete bitwidths optimizable with a gradient; and *b)* estimate surrogate gradients for these bitwidths.

1. Optimize discrete bitwidths with gradient

The first issue can be addressed by treating the discrete bitwidths similar to the discrete weights in a quantized network. In particular, we store the number of fractional bit in floating-point, and apply the STE to them as it is done for the weights during training. We follow the STE implementation used in QKeras:

$$\text{ste}(x) = x + \text{sg}([x] - x), \quad (6)$$

where the *stop gradient* operation $\text{sg} : \mathbb{R} \rightarrow \mathbb{R}$ acts as an identity function in the forward pass and a zero func-

tion in backward pass. In this way, the bitwidths can be optimized if they have gradients attached to them.

2. Surrogate gradient for bitwidths

To address the second issue, we first consider some parameter x (e.g., weight or activation) in the network and its corresponding quantizer $f^q(\cdot)$. If the number is quantized with f fractional bits, its associated quantization error δ_f can be expressed as follows:

$$\delta_f \equiv x - f^q(x) = x - \lfloor x \cdot 2^f \rfloor \cdot 2^{-f}. \quad (7)$$

During training, we assume x to be a random variable following some smooth distribution \mathbb{D}_x . We further assume that the variance of \mathbb{D}_x is significantly larger than the quantization error δ_f in such a way that one can view the quantization error's distribution as an uniform distribution:

$$\delta_f \sim \text{Uniform}(-2^{-f-1}, 2^{-f-1}). \quad (8)$$

Let the loss of the network be \mathcal{L} , and express the gradient of f with respect to \mathcal{L} as

$$\frac{\partial \mathcal{L}}{\partial f} = \frac{\partial \mathcal{L}}{\partial \delta_f} \cdot \frac{\partial \delta_f}{\partial f}. \quad (9)$$

In this expression, the first term $\frac{\partial \mathcal{L}}{\partial \delta_f}$ can be obtained trivially with backpropagation. The second term $\frac{\partial \delta_f}{\partial f}$ is not well-defined, as f can only take integer values for a properly defined quantizer and thus has no gradient. As a solution to this, we propose a surrogate gradient method that assigns a gradient to f only on integer values.

We now express the loss as a function of the weights θ and all the quantization errors δ , $\mathcal{L}(\theta, \delta)$. We further assume that the loss function is sensitive to the magnitude of the quantization errors, but not the signs, i.e. $\mathcal{L}(\theta, |\delta|)$ with $|\delta|$ being the element-wise absolute value of δ .

For a parameter $x \sim \mathcal{D}_x$ to be quantized with $f \in \mathbb{Z}$ fractional bits, the corresponding absolute quantization error is $|\delta_f| \equiv |x - f^q(x)| \sim \text{Uniform}(0, 2^{-f-1})$. By increasing f by one, we obtain the absolute quantization error $|\delta_{f+1}|$ as a function of f and $|\delta_f|$:

$$|\delta_{f+1}| = \begin{cases} |\delta_f| & |\delta_f| \leq 2^{-f-2} \\ 2^{-f-1} - |\delta_f| & |\delta_f| > 2^{-f-2} \end{cases}. \quad (10)$$

A straight forward way to obtain the gradient of $|\delta_f|$ with respect to f is to use the finite difference approximation

$$\frac{\partial |\delta_f|}{\partial f} \leftarrow |\delta_{f+1}| - |\delta_f|. \quad (11)$$

However, as the absolute quantization error is bounded by a geometric sequence of 2^{-f-1} , using a linear difference for approximation may be suboptimal. Instead, we use the following heuristic expression to approximate the gradient, which recovers Eq. (11) at the limit of $|\delta_{f+1}| \rightarrow |\delta_f|$:

$$\frac{\partial |\delta_f|}{\partial f} \leftarrow \log \frac{|\delta_{f+1}|}{|\delta_f|} \cdot |\delta_f|. \quad (12)$$

Expressing the ratio of $|\delta_{f+1}|$ and $|\delta_f|$ as a function of $|\delta_f|$, we have

$$\frac{|\delta_{f+1}|}{|\delta_f|} = \begin{cases} 1 & |\delta_f| \leq 2^{-f-2} \\ \frac{2^{-f-1}}{|\delta_f|} - 1 & |\delta_f| > 2^{-f-2} \end{cases}. \quad (13)$$

Though one may get a surrogate gradient by combining Eq. (12) and Eq. (13), the using the local relations as expressed in Eq. (13) between $|\delta_{f+1}|$ and $|\delta_f|$ would lead to a loss (gradient) landscape for f with extensive high-frequency components that is hard to optimize. To mitigate this issue, we smooth out the loss (gradient) landscape by taking the expectation of the first term of Eq. (12) over $|\delta_f| \sim \text{Uniform}(0, 2^{-f-1})$:

$$\mathbb{E}_{|\delta_f|} \left[\log \frac{|\delta_{f+1}|}{|\delta_f|} \right] = -\log 2. \quad (14)$$

By substituting Eq. (14) into Eq. (12), and add a $\text{sign}(\delta_f)$ term on both hand sides, we have

$$\frac{\partial \delta_f}{\partial f} \leftarrow -\log 2 \cdot \delta_f. \quad (15)$$

Hence, the forward pass of the quantizer, with respect to one input value x and its fractional bitwidth f , can be expressed as in Algorithm 1. The backward pass is the auto-differentiation of the forward pass with the stop-gradient operations.

Algorithm 1: Quantizer forward pass

Data: x : the input value; f : the fractional bitwidth

Result: x^q : the differentiable, quantized value of x with fractional bitwidth f_{fp}

$f \leftarrow \text{ste}(f_{fp});$

$x^q \leftarrow \text{sg}(\lfloor x \cdot 2^f \rfloor \cdot 2^{-f});$

$\delta \leftarrow \text{sg}(x - x^q);$

$\delta \leftarrow \text{sg}(\delta + \ln 2 \cdot f \cdot \delta) - \ln 2 \cdot f \cdot \delta;$

$x^q \leftarrow x - \delta;$

return x^q

As quantization results in higher loss values in general, the gradients propagated from the loss function to the bitwidths tend to increase them. To optimize for the on-chip resource usage and latency, we introduce regularization terms that encourage for smaller bitwidths.

EBOPs introduced in Section III C provides a good resource estimation. However, as it involves non-differentiable bit-counting for the weights and requires the min/max of the intermediate values in the network to be known, it cannot be directly used during training. Instead, we use $\overline{\text{EBOPs}}$, an approximated form of EBOPs computed with estimated bitwidths, as the regularization terms during training. In particular, we use $\max(i' + f, 0)$ as the bitwidths for both weights and bias to evaluate $\overline{\text{EBOPs}}$ during training.

To evaluate the integer bitwidth without the sign bit i' during training for some activations' bitwidth, we utilize the min/max values realized by the corresponding activations within the same epoch, and evaluate i' with Eq. (3). For the weights, i' is also evaluated by Eq. (3), but with the min/max values being the minimum and maximum weights corresponding to it. With f being directly available during training, we can evaluate the approximated bitwidth and compute $\overline{\text{EBOPs}}$ for each training step. Indeed, $\overline{\text{EBOPs}}$ is the upper bound of EBOPs if the min/max values used are accurate, as f serves as the upper bound of the actual number of fractional bits enclosed by non-zero bits.

$\overline{\text{EBOPs}}$ is incorporated to the loss function with as a regularization term with a coefficient $\beta \in \mathbb{R}_+$ to balance the trade-off between the model performance and on-chip resource usage. Moreover, as there are values in networks that are not involved in any multiplicative operations, such as the last-layer's outputs or inputs to non-linear activations, we apply another L-1 regularization with a coefficient $\gamma \in \mathbb{R}_+$ to the bitwidths to keep them from growing indefinitely and consuming excessive resources. Hence, the final loss function is given by

$$\mathcal{L} = \mathcal{L}_{\text{base}} + \beta \cdot \overline{\text{EBOPs}} + \gamma \cdot \text{L1}_{\text{norm}}, \quad (16)$$

with the surrogate gradients from the loss function directed attached to the bitwidths as described in Algorithm 1.

As all additional gradients introduced in this section only apply to the bitwidths, the loss landscape of the network's weights remains unperturbed compared to that of networks with static quantization parameters.

3. Gradient for bitwidths with multiple parameters

Denote the collection of parameters sharing the same bitwidth a parameter group, \mathbf{g} . In experiments, we noticed that if we increase the size of a parameter group while keeping the same β , the corresponding bitwidth is more likely to collapse to zero. To mitigate this, we normalize the gradient from the regularization terms on f by $1/\sqrt{|\mathbf{g}|}$ based on empirical observations. Here, $|\mathbf{g}|$ denotes the number of parameters in \mathbf{g} . This normalization makes the optimization more stable with respect to the size of the parameter groups.

4. Connection to Pruning

From Eq. (4), it is observable that the quantized value is constantly zero if $-\epsilon \cdot 2^{-f} \leq x < (1-\epsilon) \cdot 2^{-f}$, or equivalently, $|x| < 2^{-f-1}$ when $\epsilon = \frac{1}{2}$. As $f \in \mathbb{Z}$, a sufficiently small f will cause the corresponding parameters in the network to be constantly zero, which is equivalent to have those parameters pruned. Assigning a distinct bitwidth to each parameter group in the network through HGQ thus automatically prunes the network during training in such a way that takes both model performance and resource consumption into account. When the granularity for quantization is set to per-parameter, a fully unstructured pruning is automatically performed.

Listing 1. Keras model example

```
from tensorflow.keras.layers import Input, Dense

inp = Input((16,))
out = Dense(64, activation='relu')(out)
out = Dense(32, activation='relu')(out)
out = Dense(32, activation='relu')(out)
out = Dense(5, activation='linear')(out)

keras_model = Model(inp, out)
```

Listing 2. HGQ model example

```
from tensorflow.keras.layers import Input
from HGQ import HQuantize, HDense

inp = Input((16,))
out = HQuantize(name='inp_q', beta=beta)(out)
out = HDense(64, activation='relu', beta=beta)(out)
out = HDense(32, activation='relu', beta=beta)(out)
out = HDense(32, activation='relu', beta=beta)(out)
out = HDense(5, activation='linear', beta=beta)(out)

hgq_model = Model(inp, out)
```

IV. THE HIGH GRANULARITY QUANTIZATION FRAMEWORK

The HGQ algorithm is available as a user-friendly Python library similar to `QKeras`. It functions as an advanced quantization API built on top of `Keras`, while leveraging `hls4ml` for the downstream model deployment on chips. This framework facilitates automatic conversion of `keras` models into `hls4ml` models, ensuring bit-accuracy as per the specifications of a dataset defined by the user without requiring any further manual configuration.

HGQ is engineered to carry out automatic quantization on all compatible layers according to the $\overline{\text{EBOPs}}$ regularization factor, β , and the L-1 regularization factor, γ . This approach eliminates the necessity for users to fine-tune quantization parameters for individual modules or undergo multiple training cycles to identify the best quantization scheme.

The HGQ framework provides drop-in replacements for the most commonly used `Keras` layers, making it straightforward to rewrite a standard `Keras` model to

an HGQ model with minimal adjustments. For instance, as demonstrated in Listing 1 and 2, converting a `Keras` model to its HGQ counterpart primarily involves substituting existing layers with their HGQ alternatives, along with the inclusion of an additional layer to quantize the input values. The HGQ framework provides two categories of layers: Heterogeneous (H-) layers, which accept an additional parameter, `beta`, to manage the layer’s resource usage regularization strength based on $\overline{\text{EBOPs}}$, and Passive (P-) layers, which serve to relay metadata without performing quantization. The H- layers also allow for layer-specific kernel and activation quantizer configurations for more fine-grained controls. Though manual bitwidth configuration should not be required in most cases, the user may still opt to specify the bitwidths for specific layers if necessary.

Beyond quantization-aware training, the framework introduces a convenient intermediate model representation, “proxy models” for converting a trained `Keras` model to a `hls4ml` project. This feature accommodates both HGQ and `qKeras` models, automating the creation and enforcement of the `hls4ml`’s quantization configurations for precise conversions. Furthermore, the proxy model facilitates bit-accurate emulation of the compiled `hls4ml` model, aiding in debugging and validating the `hls4ml` model’s performance before development. As this emulation correctly models the overflow behavior of the fixed-point numbers, it is still accurate in case of overflows due to limited bitwidths. Though, when the intermediate values are quantized with a high bitwidth, the emulation may have errors at machine epsilon level due to the use of floating-point numbers in the emulation.

V. RESULTS

To evaluate the performance of the HGQ method, we train and evaluate models on two classification tasks – one for physics experiment and one for computer vision – and one regression task for physics experiment: jet tagging at the LHC [36], SVHN digit classification [64], and muon tracking at the LHC [65], respectively.

To demonstrate the trade-off between the accuracy (or resolution for regression tasks) and resource usage of the models, we methodically adjusted the β factor for each task during training to map out the Pareto Fronts. For each training run, we initialize all layers with a notably small β , which is then gradually increased through the training. Meanwhile, we maintained the γ value fixed at $2 \cdot e^{-6}$ for all experiments to avert the risk of diverging bitwidths for some parameters.

After each epoch, we record the validation accuracy (or resolution) and $\overline{\text{EBOPs}}$, and maintain all model’s checkpoints that are on the Pareto Front defined by these two metrics. Post-training, we use the entire training and validation sets as the calibration dataset to determine the required bitwidths and evaluate the exact EBOPs for all checkpointed models. Subsequently, we compute the test

accuracy (resolution) for all the models, and then obtain their on-chip resource consumptions after performing the place-and-route phase with Vivado/Vitis[®].

A. Resource Estimation via EBOPs

We first demonstrate that EBOPs is a good estimator for on-chip resource consumption. We consider these types of major resources on an AMD[®] FPGA chip: flip-flops (FFs, sometime referred to as registers), LUTs, DSPs, and onboard memories (BRAMs and URAMs). When designing an unrolled neural network for ultra low latency applications like the hardware triggers for LHC experiments, the limiting resources are usually either LUTs or DSPs. Empirically, for models synthesized with Vivado/Vitis[®] HLS, operations consisting of larger bitwidths are more likely to consume DSPs, while operations with smaller bitwidths are more likely to consume LUTs. In our experiments, we observed that the EBOPs roughly predict a linear combination of the LUTs and DSPs consumption, namely, $\text{EBOP} \approx \text{LUT} + 55 \times \text{DSP}$ for models synthesized with parallel IO, i.e., intermediate values in the model are directly wired between layers/modules with no extra buffer in between.

In Figure II, we demonstrate this relationship between EBOPs and the actual on-chip resource consumption. Data points shown in this figure are from the models presented later in this section for the aforementioned three tasks. Although the relationship is not exact, we can still make a reasonable estimation of the resource usage based on EBOPs. Also, this linear relation suggests that treating one DSP as approximately 55 LUTs could be a practical approximation when comparing resource usage across different models. It is important to note that EBOPs primarily account for operations involving vector dot product-like operations between constants and variables. Therefore, if other kind of operations significantly contribute to the on-chip resource consumption, EBOPs will underestimate the overall resource consumption. For instance, the SVHN classifier models shown in Figure II synthesized with stream IO, which requires additional buffers for intermediate values, have higher actual resource consumptions than what EBOPs predicts.

B. Jet Classification at the LHC

We conducted a comparison of the classification accuracy, latency, and on-chip resource utilization of models trained with HGQ against various quantized models from earlier researches for this task.

We use the dataset from [68] to classify jets – collimated showers of particles from quark and gluon decay at collider physics experiments – into five classes based on their originating particle: single quark (q), single gluon (g), W and Z bosons decaying to two quarks, and top (t) quark decaying to two quarks and a heavier bottom

TABLE I. Accuracy, resource consumption, latency, and initiation intervals (IIs) of the jet tagging models. Resource reported for **HGQ** models are after place-and-route with an AMD[®] Virtex[®] UltraScale+™ XCVU9P FPGA. **HGQ** models outperforms the baseline models by a large margin in all accuracy, resource consumption, and latency.

Model	Accuracy (%)	Latency (cc)	DSP (%)	LUT (%)	FF (%)	II (cc)
BF [36]	74.4	9 (45 ns)	56.0 (1,826)	4.09 (48,321)	0.8 (20,132)	1
BP [36]	74.8	14 (70 ns)	7.7 (526)	1.49 (17,577)	0.4 (10,548)	1
BH [36]	73.2	14 (70 ns)	1.3 (88)	1.34 (15,802)	0.3 (8,108)	1
Q6 [36]	74.8	11 (55 ns)	1.8 (124)	3.36 (39,782)	0.3 (8,128)	1
QE [36]	72.3	11 (55 ns)	1.0 (66)	0.77 (9,149)	0.1 (1,781)	1
QB [36]	71.9	14 (70 ns)	1.0 (69)	0.95 (11,193)	0.1 (1,771)	1
LogicNets JSC-M [66]	70.6	N/A	0 (0)	1.22 (14,428)	0.02 (440)	1
LogicNets JSC-L [66]	71.8	5 (13 ns)	0 (0)	3.21 (37,931)	0.03 (810)	1
BP-DSP-RF=2 [45]	76.3	21 (105 ns)	2.6 (175)	0.47 (5,504)	0.13 (3,036)	2
MetaML- $\alpha_q=1\%$ [37]	75.6	9 (45 ns)	0.7 (50)	0.57 (6,698)	N/A	1
MetaML- $\alpha_q=4\%$ [37]	72.8	8 (40 ns)	0.2 (23)	0.57 (7,224)	N/A	1
SymbolNet [67]	71.	2 (10 ns)	<0.1 (3)	0.01 (177)	<0.01 (109)	1
HGQ-1	76.4	6 (30 ns)	0.50 (34)	0.53 (6,236)	0.05 (1253)	1
HGQ-2	75.9	4 (20 ns)	0.09 (6)	0.27 (3,162)	0.02 (550)	1
HGQ-3	75.0	4 (20 ns)	0.07 (5)	0.13 (1,540)	0.02 (370)	1
HGQ-4	73.9	3 (15 ns)	0.00 (0)	0.05 (565)	0.01 (140)	1
HGQ-5	72.5	2 (10 ns)	0.00 (0)	0.04 (468)	0.01 (131)	1
HGQ-6	71.0	2 (10 ns)	0.00 (0)	0.02 (256)	0.00 (66)	1
HGQ-c1	76.3	8 (40 ns)	0.26 (18)	0.50 (5,899)	0.09 (2,072)	1
HGQ-c2	74.2	3 (15 ns)	0.00 (0)	0.06 (678)	0.01 (172)	1

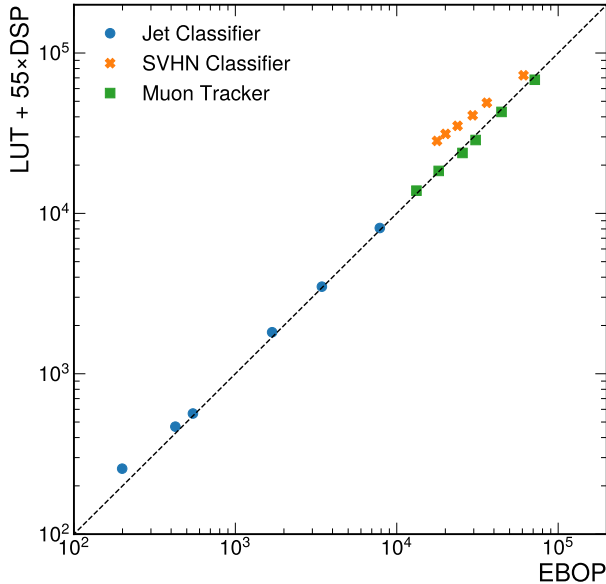


FIG. II. The relationship between EBOPs and the post place-and-route resource consumption. Data points shown in this figure are from models presented later in this section for the three tasks. The EBOPs roughly predicts a linear combination of the LUTs and DSPs consumption for models synthesized with parallel IO.

quark. The inputs for each jet are 16 scalar values representing physics-motivated high-level features. The model architecture employed is based on the full precision baseline model described in the original work [36], which is a 4-layer fully connected neural network.

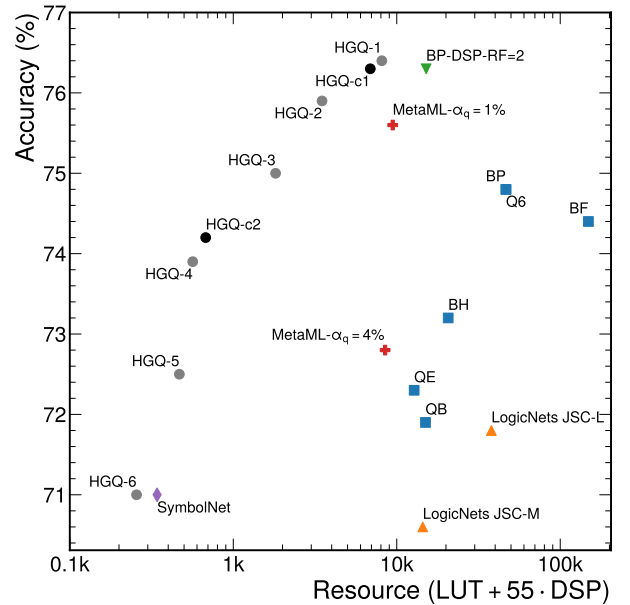


FIG. III. Accuracy versus resource consumptions of the jet tagging models. Note that models with different DSP and LUT usage could land on the same point on this plot due to the linear combination of DSPs and LUTs.

We summarize the performance and resource usage of all models we compared in Table I and visualize them in Figure III. The following models shown are cited from [36]: Baseline Full (BF), Baseline Pruned (BP), Baseline Heterogeneous (BH), Quantized 6-bit (Q6), AutoQKeras Energy Optimized (QE), and AutoQKeras Bits Optimized (QB) models. All of these models, except

for BF and BP, are trained quantization-aware. Hyperparameter optimizations with Gaussian Process are applied to the AutoQKeras models to achieve low resource consumption. LogicNets JSC-M and JSC-L are cited from [66], where the networks are co-designed to use on-chip LUTs efficiently. BP-DSP-RF=2 [45] is a neural network implemented in QKeras with a reuse factor (i.e., how many times a multiplier logic unit may be used for inferencing one sample) of two, which is pruned to reduce DSP usage while preserving accuracy by formulating the trade-off as a knapsack problem. For MetaML- $\alpha_q=1\%$ and MetaML- $\alpha_q=4\%$ [37], iterative searches through model architecture and quantization/pruning configurations are performed to achieve better accuracy-resource trade-offs. SymbolNet [67] leverages a gradient-based method for neural symbolic regression. It also uses an adaptive dynamic pruning scheme to reduce on-chip resource consumption while maintaining the accuracy.

The HGQ trained models, HGQ 1 through 6, are taken from the same training in which β is gradually increased. The model is initialized with 2 fractional bits for activations, and a bitwidth of 2 excluding the sign bit for the weights. This model is fully unrolled, and per-parameter quantization is applied. Throughout the training process of 300,000 epochs, β is gradually increased from 10^{-6} to 10^{-4} . Due to the model’s compact size, the entire training completes in ~ 4 hours on a modern consumer GPU with a batch size of 33,200.

As shown in Figure III and Table I, the HGQ approach outperforms all previous works on quantized neural networks by significant margins, both in terms of model accuracy and resource usage. Depending on the working point, HGQ may reduce the resource consumption from 50% to up to 95% while maintaining the same accuracy. When working with a lower accuracy requirement, HGQ could also achieve similar resource consumption to an optimized symbolic classifier.

We also studied the performance of the HGQ models trained with fixed β values. In Figure III and Table I, these correspond to **HGQ-c1** and **HGQ-c2**, which are trained with fixed β ’s of $2.1e-6$ and $1.2e-5$, respectively. Both models are trained for 5,000 epochs with the same batch size. By comparing with the forementioned HGQ models, we observe that models trained with either a constant or increasing β value achieved comparable balance between accuracy and resource consumption. This suggests that a lengthy training process with a gradually increasing β value is not always necessary for using HGQ to obtain optimal trade-offs between accuracy and resource efficiency.

C. SVHN Classifier

We also benchmark HGQ on a computer vision task and compare it to previous state-of-the-art works [45, 64] on real-time inferences. We make use of the SVHN dataset [69] which consists of 32×32 RGB images of house

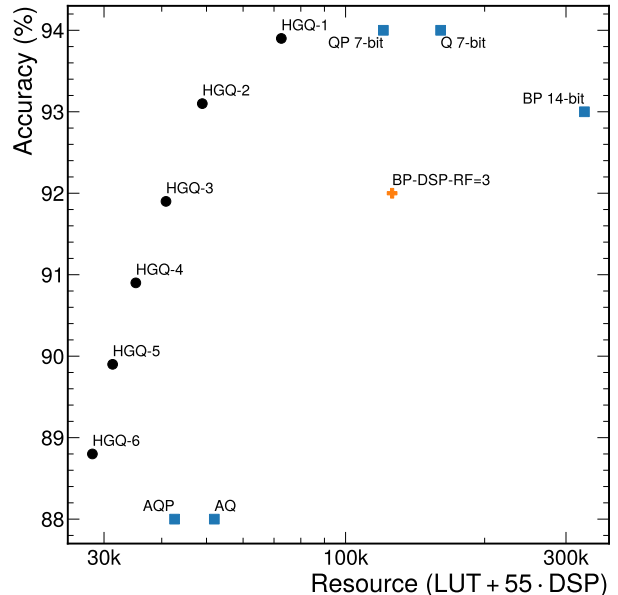


FIG. IV. Accuracy versus resource consumptions of the SVHN classifier models. Note that models with different DSP and LUT consumption could land on the same point on this plot due to taking a linear combination of DSPs and LUTs.

numbers taken from Google Street View, and the task is to classify the digit in the center of the image into one of ten classes. The architecture of the model is a LeNet-like [70], convolution-dense network taken from [64].

We summarize the performance and resource usage of all models we compared in Table II and visualize them in Figure IV. In the table and figure, AutoQkeras Pruned (AQP), AutoQkeras (AQ), QKeras Pruned 7-bit (QP 7-bit), QKeras 7-bit (Q 7-bit), and Baseline Pruned (BP 14-bit) are taken from [64]. All of these models except BP are trained quantization aware with QKeras. In particular, AQP, QP, and BP are pruned to a sparsity of 50% iteratively with a magnitude-based method during training. AQP and AQ are heterogeneously quantized models, where the quantization configurations are optimized through AutoQKeras’s hyperparameter tuner with Gaussian Process. BP-DSP-RF=3 is cited from [45], where the network is implemented in QKeras with a reuse factor of three, and it formulates the trade-off between accuracy and DSP usage as a snappack problem to perform optimal pruning.

The HGQ trained models, HGQ 1 though 6, are taken from a single training run during which the β value is gradually increased. For training, we initialize the model with 6 fractional bits for activations, and a bitwidth of 6 for weights excluding the sign bit. The β value is systematically increased from 10^{-7} to 10^{-4} over approximately 12,000 epochs. Completing this training process requires ~ 10 hours on a modern consumer GPU with a batch size of 2,048.

As this model is too large to fit on-chip if fully unrolled, we use the stream IO implementation in `hls4ml`. This

TABLE II. Accuracy, resource usage, latency, and initiation intervals of the SVHN classifier models. Reported resource usage for **HGQ** models are after place-and-route with an AMD[®] Virtex[®] UltraScale+™ XCVU9P FPGA. **HGQ** models outperforms the baseline models both in accuracy and resource consumption while maintaining comparable latency.

Model	Accuracy (%)	Latency (cc)	DSP (%)	LUT (%)	FF (%)	BRAM (%)	II (cc)
BP 14-bit [64]	93.	1,035 (5.18 μ s)	48.85 (3,341)	12.27 (145,089)	2.77 (65,482)	3.08 (66.5)	1,030
Q 7-bit [64]	94.	1,034 (5.17 μ s)	2.56 (175)	12.77 (150,981)	1.51 (35,628)	3.10 (67.0)	1,029
QP 7-bit [64]	94.	1,035 (5.18 μ s)	2.54 (174)	9.40 (111,152)	1.38 (32,554)	3.10 (67.0)	1,030
AQ [64]	88.	1,059 (5.30 μ s)	1.05 (72)	4.06 (48,027)	0.64 (15,242)	1.48 (32.5)	1,029
AQP [64]	88.	1,059 (5.30 μ s)	1.02 (70)	3.28 (38,795)	0.63 (14,802)	1.39 (30.5)	1,029
BP-DSP-RF=3 [45]	92.	? (43.58 μ s)	17.76 (1,215)	5.01 (59,279)	1.97 (46,584)	35.88 (1,550)	35.88
HGQ-1	93.9	1050 (5.25 μ s)	0.85 (58)	5.87 (69,407)	1.18 (27853)	1.48 (32.0)	1029
HGQ-2	93.1	1061 (5.31 μ s)	0.44 (30)	4.00 (47,314)	0.87 (20582)	1.30 (28.0)	1029
HGQ-3	91.9	1058 (5.29 μ s)	0.22 (15)	3.39 (40,032)	0.76 (18087)	1.09 (23.5)	1029
HGQ-4	90.9	1059 (5.30 μ s)	0.19 (13)	2.91 (34,435)	0.73 (17261)	1.04 (22.5)	1029
HGQ-5	89.9	1056 (5.28 μ s)	0.15 (10)	2.60 (30,766)	0.64 (15205)	0.97 (21.0)	1029
HGQ-6	88.8	1056 (5.28 μ s)	0.09 (6)	2.37 (27,982)	0.62 (14736)	0.97 (21.0)	1029

partitions the convolutional layers into smaller blocks by individual kernel operations (i.e., partitioned by rows in the im2col algorithm [71]) and compute them once at a time at inference time [64]. Due to limitations of the current implementation, intra-layer heterogeneous activation quantization cannot be utilized with stream IO. Hence, while the weights are quantized at the per-parameter granularity, activations are quantized in layer-wise blocks. Nevertheless, HGQ still outperforms both baselines by a considerable margin of up to 40% in resource savings while maintaining similar accuracy and latency.

D. Muon Tracker

For this task, we compare the resolution, latency, and on-chip resource consumption of the HGQ trained models to models presented in [65] on a regression task proposed in the same work. The task involves predicting the incidence angle of a simulated muon track in a particle detector. The inputs are one 3×50 and two 3×50 binary-valued arrays, representing the hits recorded in three detector stations. The output is a single scalar value representing the angle in milliradians. We evaluate the network’s performance in resolution, defined by the root-mean-square of the angle’s reconstruction errors. Following the same approach in [65], we exclude outliers where the absolute error is greater than 30 milliradians. The architecture of the model is a multistage neural network taken from the original work.

The results, including the performance and resource consumption of the models trained with HGQ and the models proposed in the original work, are presented in Table III and visualized in Figure V. The Quantized with * fractional bits (Qf*) models presented in [65] are all trained quantization aware with QKeras using manually tuned parameters, where * stands for the number of fractional bits used in all network parameters.

The HGQ trained models, HGQ 1 though 6, are taken from a single training run during which the β value is

gradually increased. We initialize the model with 6 fractional bits for activations, and a bitwidth of 6 excluding the sign bit for the weights. The model is fully unrolled, and the quantization is applied at the per-parameter granularity. The β value is systematically increased from $3 \cdot e-6$ to $6 \cdot e-4$ over approximately 600,000 epochs, which takes ~ 16 hours on a modern consumer GPU with a batch size of 16,384.

The HGQ models consistently outperform the baseline models with a reduction in resource consumption of 40 \sim 50%, while achieving the same or better resolution with comparable latency.

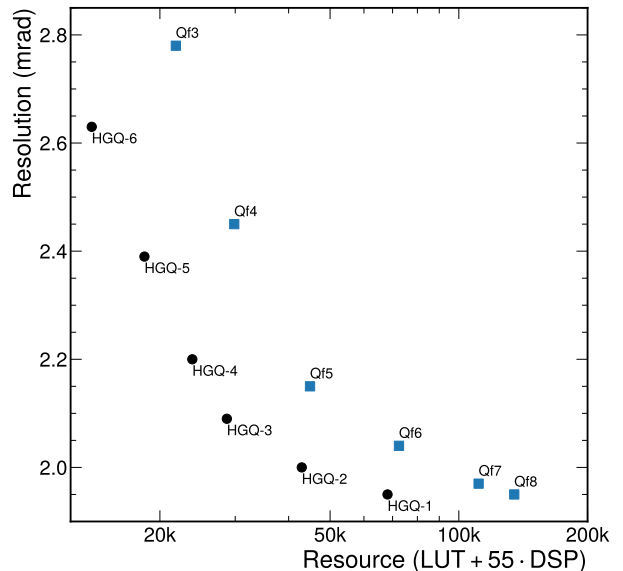


FIG. V. Resolution versus resource consumptions of the muon tracking models. Note that models with different DSP and LUT consumption could land on the same point on this plot as a result of taking the linear combination of DSPs and LUTs.

TABLE III. Resolution, resource consumption, latency, and initiation intervals of the Muon Tracker models. The resource usage reported for **HGQ** models are after place-and-route with an AMD[®] Virtex[®] UltraScale+™ XCVU13P FPGA. **HGQ** models outperforms the baseline models both accuracy and resource consumption for this task while maintaining comparable latency.

Model	Resolution (mrad)	Latency (cc)	DSP (%)	LUT (%)	FF (%)	BRAM (%)	II (cc)
Qf8 [65]	1.95	17 (106.3 ns)	14.34 (1,762)	2.19 (37,867)	0.24 (8,443)	1.40 (37.5)	1
Qf7 [65]	1.97	11 (68.8 ns)	11.30 (1,389)	2.02 (34,848)	0.16 (5,433)	1.40 (37.5)	1
Qf6 [65]	2.04	13 (81.3 ns)	2.64 (324)	3.16 (54,638)	0.19 (6,525)	1.40 (37.5)	1
Qf5 [65]	2.15	11 (68.8 ns)	0.72 (88)	2.32 (40,039)	0.10 (3,419)	1.40 (37.5)	1
Qf4 [65]	2.45	10 (62.5 ns)	0.20 (24)	1.65 (28,526)	0.09 (2,954)	1.40 (37.5)	1
Qf3 [65]	2.78	9 (56.3 ns)	0.02 (2)	1.25 (21,682)	0.06 (2,242)	1.40 (37.5)	1
HGQ-1	1.95	11 (68.8 ns)	4.25 (522)	2.28 (39,413)	0.17 (6,043)	0.93 (25.0)	1
HGQ-2	2.00	11 (68.8 ns)	1.25 (154)	1.99 (34,460)	0.15 (5,263)	0.93 (25.0)	1
HGQ-3	2.09	12 (75.0 ns)	0.55 (68)	1.44 (24,941)	0.14 (4,677)	1.40 (37.5)	1
HGQ-4	2.20	13 (81.3 ns)	0.33 (41)	1.25 (21,557)	0.14 (4,699)	1.40 (37.5)	1
HGQ-5	2.39	10 (62.5 ns)	0.22 (27)	0.98 (16,918)	0.07 (2,484)	1.40 (37.5)	1
HGQ-6	2.63	12 (75.0 ns)	0.08 (10)	0.77 (13,306)	0.10 (3,429)	0.93 (25.0)	1

VI. CONCLUSION AND FUTURE WORK

In this work, we present HGQ, a novel method to optimize quantized neural networks for real-time applications on FPGAs and possibly also ASICs. The HGQ approach enables the optimization of the quantization bitwidths at arbitrary granularity, up to per-parameter level, through a gradient-based approach that is conscious of both resource usage and loss minimization. By maximally leveraging the ability of the specialized hardware to perform fully heterogeneous computations, we are able to minimize the resource consumption by the models while maintaining the model performance. In particular, our findings show that HGQ achieves up to a 95% reduction in resource consumption compared to leading compression techniques on FPGAs without performance degradation. We further demonstrate that a single training session with HGQ is sufficient to explore a broad spectrum of trade-offs between model performance and resource utilization, efficiently recovering the Pareto Frontier, thereby rendering the model optimization process both more efficient and effective. Moreover, we introduce EBOPs, a metric providing an accurate estimation of the final on-chip resource consumption of a model as a linear combination of LUTs and DSPs, allowing for efficient software-hardware co-designs.

To facilitate adoption, we have developed a user-friendly library that simplifies the application of this method. The library offers an easy-to-use interface for defining and training of quantized neural networks with our method. Through interfacing with `hls4ml`, HGQ provides bit-accurate conversions from software to FPGA firmware models without the need of manual intervention, significantly simplifying and streamlining the work-

flow from training to deployment.

We are looking forward to developing new neural networks based triggers for the CERN LHC experiments, with the HGQ+hls4ml workflow for the incoming data taking period. With the increased hardware efficiency, we hope to enable more complex models to be deployed on the trigger system, which could lead to more accurate trigger decisions. For future improvements of this method, we hope to develop a differential latency estimator for the models. Though lower bitwidths generally result in lower latencies, this relation does not hold in some cases, like when the HLS backend switches between DSP and LUT based arithmetic implementations. Also, we would like to explore the possibility of having separate LUT and DSP consumption estimators, as the resource constraints of the two are not always interchangeable depending on the specific application.

VII. ACKNOWLEDGEMENTS

C.S. is partially supported by the Caltech Danny Koh grad fellowship. C.S. acknowledges partial support from Günther Dissertori. C.S. and M.S. acknowledge partial support from the U.S. Department of Energy (DOE), Office of Science, Office of High Energy Physics grant DE-SC0011925. T.Å. is supported by the Swiss National Science Foundation Grant No. PZ00P2_201594. J.N., M.S., and C.S. are partially supported by the U.S. Department of Energy (DOE), Office of Science, Office of High Energy Physics “Designing efficient edge AI with physics phenomena” Project (DE-FOA-0002705). J.N. is partially supported by the AI2050 program at Schmidt Futures (Grant G-23-64934). V.L. is supported by the NSF Institute for Accelerated AI Algorithms for Data-Driven Discovery (A3D3), under the NSF grant #PHY-2117997.

[1] Singh, R. & Gill, S. S. Edge ai: A survey. *Internet of Things and Cyber-Physical Systems* **3**, 71–

92 (2023). URL <https://www.sciencedirect.com/>

- [science/article/pii/S2667345223000196](https://doi.org/10.1109/TPAMI.2021.3089687).
- [2] Niu, W. *et al.* Grim: A general, real-time deep learning inference framework for mobile devices based on fine-grained structured weight sparsity. *IEEE Trans. Pattern Anal. Mach. Intell.* **44**, 6224–6239 (2022). URL <https://doi.org/10.1109/TPAMI.2021.3089687>.
 - [3] Huang, K. & Gao, W. Real-time neural network inference on extremely weak devices: agile offloading with explainable ai. In *Proceedings of the 28th Annual International Conference on Mobile Computing And Networking*, MobiCom '22, 200–213 (Association for Computing Machinery, New York, NY, USA, 2022). URL <https://doi.org/10.1145/3495243.3560551>.
 - [4] Yang, Y. *et al.* Streamvc: Real-time low-latency voice conversion (2024). URL https://google-research.github.io/seanet/stream_vc/.
 - [5] The LHC Study Group. The Large Hadron Collider, Conceptual Design. Tech. Rep., CERN/AC/95-05 (LHC) Geneva (1995).
 - [6] The CMS Collaboration. The Phase-2 Upgrade of the CMS Level-1 Trigger. Tech. Rep., CERN, Geneva (2020). URL <https://cds.cern.ch/record/2714892>. Final version.
 - [7] The ATLAS Collaboration. Technical Design Report for the Phase-II Upgrade of the ATLAS TDAQ System. Tech. Rep., CERN, Geneva (2017). URL <https://cds.cern.ch/record/2285584>.
 - [8] Zurbano Fernandez, I. *et al.* High-Luminosity Large Hadron Collider (HL-LHC): Technical design report. *CERN Yellow Reports: Monographs* **10/2020** (2020).
 - [9] Menghani, G. Efficient deep learning: A survey on making deep learning models smaller, faster, and better. *ACM Computing Surveys* **55**, 1 – 37 (2021). URL <https://api.semanticscholar.org/CorpusID:235446458>.
 - [10] Li, Z., Li, H. & Meng, L. Model compression for deep neural networks: A survey. *Computers* **12** (2023). URL <https://www.mdpi.com/2073-431X/12/3/60>.
 - [11] Abadi, M. *et al.* TensorFlow: Large-scale machine learning on heterogeneous systems (2015). URL <https://www.tensorflow.org/>. Software available from tensorflow.org.
 - [12] Chollet, F. *et al.* Keras. <https://keras.io> (2015).
 - [13] Duarte, J. *et al.* Fast inference of deep neural networks in FPGAs for particle physics. *Journal of Instrumentation* **13**, P07027–P07027 (2018). URL <https://doi.org/10.1088/1748-0221/13/07/p07027>.
 - [14] <https://github.com/fastmachinelearning/hls4ml>.
 - [15] <https://github.com/calad0i/HGQ>.
 - [16] Zhou, S. *et al.* Dorefa-net: Training low bitwidth convolutional neural networks with low bitwidth gradients. *CoRR abs/1606.06160* (2016). URL <http://arxiv.org/abs/1606.06160>. 1606.06160.
 - [17] Lin, X., Zhao, C. & Pan, W. Towards accurate binary convolutional neural network. In Guyon, I. *et al.* (eds.) *Advances in Neural Information Processing Systems*, vol. 30 (Curran Associates, Inc., 2017). URL https://proceedings.neurips.cc/paper_files/paper/2017/file/b1a59b315fc9a3002ce38bbe070ec3f5-Paper.pdf.
 - [18] Courbariaux, M., Bengio, Y. & David, J. Binaryconnect: Training deep neural networks with binary weights during propagations. *CoRR abs/1511.00363* (2015). URL <http://arxiv.org/abs/1511.00363>. 1511.00363.
 - [19] Rastegari, M., Ordonez, V., Redmon, J. & Farhadi, A. Xnor-net: Imagenet classification using binary convolutional neural networks. In Leibe, B., Matas, J., Sbebe, N. & Welling, M. (eds.) *Computer Vision – ECCV 2016*, 525–542 (Springer International Publishing, Cham, 2016).
 - [20] Li, F., Liu, B., Wang, X., Zhang, B. & Yan, J. Ternary weight networks (2022). 1605.04711.
 - [21] Zhu, C., Han, S., Mao, H. & Dally, W. J. Trained ternary quantization (2017). 1612.01064.
 - [22] He, Z. & Fan, D. Simultaneously optimizing weight and quantizer of ternary neural network using truncated gaussian approximation. *2019 IEEE/CVF Conference on Computer Vision and Pattern Recognition (CVPR)* 11430–11438 (2018).
 - [23] Xu, C. *et al.* Alternating multi-bit quantization for recurrent neural networks. *CoRR abs/1802.00150* (2018). URL <http://arxiv.org/abs/1802.00150>. 1802.00150.
 - [24] Guo, Y., Yao, A., Zhao, H. & Chen, Y. Network sketching: Exploiting binary structure in deep cnns. *CoRR abs/1706.02021* (2017). URL <http://arxiv.org/abs/1706.02021>. 1706.02021.
 - [25] Zhang, D., Yang, J., Ye, D. & Hua, G. Lq-nets: Learned quantization for highly accurate and compact deep neural networks. *CoRR abs/1807.10029* (2018). URL <http://arxiv.org/abs/1807.10029>. 1807.10029.
 - [26] Qu, Z., Zhou, Z., Cheng, Y. & Thiele, L. Adaptive loss-aware quantization for multi-bit networks. *CoRR abs/1912.08883* (2019). URL <http://arxiv.org/abs/1912.08883>. 1912.08883.
 - [27] Chang, S.-E. *et al.* Mix and match: A novel fpga-centric deep neural network quantization framework. In *2021 IEEE International Symposium on High-Performance Computer Architecture (HPCA)*, 208–220 (2021).
 - [28] Wang, K., Liu, Z., Lin, Y., Lin, J. & Han, S. Hardware-centric autolm for mixed-precision quantization. *International Journal of Computer Vision* **128**, 2035–2048 (2020). URL <https://doi.org/10.1007/s11263-020-01339-6>.
 - [29] Lou, Q., Guo, F., Kim, M., Liu, L. & Jiang, L. Autoq: Automated kernel-wise neural network quantization. In *International Conference on Learning Representations* (2020). URL <https://openreview.net/forum?id=rygfnm4twS>.
 - [30] Dong, Z., Yao, Z., Gholami, A., Mahoney, M. W. & Keutzer, K. HAWQ: hessian aware quantization of neural networks with mixed-precision. *CoRR abs/1905.03696* (2019). URL <http://arxiv.org/abs/1905.03696>. 1905.03696.
 - [31] Dong, Z. *et al.* HAWQ-V2: hessian aware trace-weighted quantization of neural networks. *CoRR abs/1911.03852* (2019). URL <http://arxiv.org/abs/1911.03852>. 1911.03852.
 - [32] Yao, Z., Gholami, A., Keutzer, K. & Mahoney, M. W. Pyhessian: Neural networks through the lens of the hessian. *2020 IEEE International Conference on Big Data (Big Data)* 581–590 (2019). URL <https://api.semanticscholar.org/CorpusID:209376531>.
 - [33] Choi, J. *et al.* Bridging the accuracy gap for 2-bit quantized neural networks (QNN). *CoRR abs/1807.06964* (2018). URL <http://arxiv.org/abs/1807.06964>. 1807.06964.
 - [34] Frantar, E., Singh, S. P. & Alistarh, D. Optimal brain compression: a framework for accurate post-training quantization and pruning. In *Proceedings of the 36th International Conference on Neural Information Processing*

- Systems*, NIPS '22 (Curran Associates Inc., Red Hook, NY, USA, 2024).
- [35] Wu, B. *et al.* Mixed precision quantization of convnets via differentiable neural architecture search. *CoRR abs/1812.00090* (2018). URL <http://arxiv.org/abs/1812.00090>. 1812.00090.
- [36] Coelho, C. N. *et al.* Automatic heterogeneous quantization of deep neural networks for low-latency inference on the edge for particle detectors. *Nature Machine Intelligence* **3**, 675–686 (2021). URL <https://doi.org/10.1038%2Fs42256-021-00356-5>.
- [37] Que, Z. *et al.* Metaml: Automating customizable cross-stage design-flow for deep learning acceleration. In *2023 33rd International Conference on Field-Programmable Logic and Applications (FPL)*, 248–252 (2023).
- [38] Sun, M. *et al.* Film-qnn: Efficient fpga acceleration of deep neural networks with intra-layer, mixed-precision quantization. *Proceedings of the 2022 ACM/SIGDA International Symposium on Field-Programmable Gate Arrays* (2022). URL <https://doi.org/10.1145/3490422.3502364>.
- [39] Park, E., Yoo, S. & Vajda, P. Value-aware quantization for training and inference of neural networks. In Ferrari, V., Hebert, M., Sminchisescu, C. & Weiss, Y. (eds.) *Computer Vision – ECCV 2018*, 608–624 (Springer International Publishing, Cham, 2018).
- [40] Dettmers, T., Lewis, M., Shleifer, S. & Zettlemoyer, L. 8-bit optimizers via block-wise quantization. *9th International Conference on Learning Representations, ICLR* (2022).
- [41] Dettmers, T. *et al.* Spqr: A sparse-quantized representation for near-lossless llm weight compression (2023). 2306.03078.
- [42] Kim, S. *et al.* Squeezellm: Dense-and-sparse quantization. *arXiv* (2023).
- [43] Le Cun, Y., Denker, J. S. & Solla, S. A. Optimal brain damage. In *Proceedings of the 2nd International Conference on Neural Information Processing Systems, NIPS'89*, 598–605 (MIT Press, Cambridge, MA, USA, 1989).
- [44] Hassibi, B., Stork, D. & Wolff, G. Optimal brain surgeon and general network pruning. In *IEEE International Conference on Neural Networks*, 293–299 vol.1 (1993).
- [45] Ramhorst, B., Constantinides, G. A. & Loncar, V. Fpga resource-aware structured pruning for real-time neural networks (2023). 2308.05170v1.
- [46] Meng, F. *et al.* Pruning filter in filter. In Larochelle, H., Ranzato, M., Hadsell, R., Balcan, M. & Lin, H. (eds.) *Advances in Neural Information Processing Systems*, vol. 33, 17629–17640 (Curran Associates, Inc., 2020). URL https://proceedings.neurips.cc/paper_files/paper/2020/file/ccb1d45fb76f7c5a0bf619f979c6cf36-Paper.pdf.
- [47] Li, Y. *et al.* Differentiable transportation pruning (2023). 2307.08483.
- [48] Kwon, W. *et al.* A fast post-training pruning framework for transformers. In Koyejo, S. *et al.* (eds.) *Advances in Neural Information Processing Systems*, vol. 35, 24101–24116 (Curran Associates, Inc., 2022). URL https://proceedings.neurips.cc/paper_files/paper/2022/file/987bed997ab668f91c822a09bce3ea12-Paper-Conference.pdf.
- [49] Liu, J., Xu, Z., Shi, R., Cheung, R. C. C. & So, H. K. Dynamic sparse training: Find efficient sparse network from scratch with trainable masked layers. *CoRR abs/2005.06870* (2020). URL <https://arxiv.org/abs/2005.06870>. 2005.06870.
- [50] Frantar, E. & Alistarh, D. Sparsegpt: Massive language models can be accurately pruned in one-shot (2023). 2301.00774.
- [51] Zhang, S., Wang, M., Liu, S., Chen, P.-Y. & Xiong, J. Why lottery ticket wins? a theoretical perspective of sample complexity on sparse neural networks. In Ranzato, M., Beygelzimer, A., Dauphin, Y., Liang, P. & Vaughan, J. W. (eds.) *Advances in Neural Information Processing Systems*, vol. 34, 2707–2720 (Curran Associates, Inc., 2021). URL https://proceedings.neurips.cc/paper_files/paper/2021/file/15f99f2165aa8c86c9dface16fef281-Paper.pdf.
- [52] Vischer, M. A., Lange, R. T. & Sprekeler, H. On lottery tickets and minimal task representations in deep reinforcement learning. In *International Conference on Learning Representations* (2022). URL https://openreview.net/forum?id=F13Mg_MZR-.
- [53] Frankle, J. & Carbin, M. The lottery ticket hypothesis: Finding sparse, trainable neural networks. In *International Conference on Learning Representations* (2019). URL <https://openreview.net/forum?id=rJl-b3RcF7>.
- [54] Miao, L. *et al.* Learning pruning-friendly networks via frank-wolfe: One-shot, any-sparsity, and no retraining. In *International Conference on Learning Representations* (2022). URL https://openreview.net/forum?id=01DEtITim__.
- [55] Chijiwa, D., Yamaguchi, S. y., Ida, Y., Umakoshi, K. & INOUE, T. Pruning randomly initialized neural networks with iterative randomization. In Ranzato, M., Beygelzimer, A., Dauphin, Y., Liang, P. & Vaughan, J. W. (eds.) *Advances in Neural Information Processing Systems*, vol. 34, 4503–4513 (Curran Associates, Inc., 2021). URL https://proceedings.neurips.cc/paper_files/paper/2021/file/23e582ad8087f2c03a5a31c125123f9a-Paper.pdf.
- [56] Zhou, A. *et al.* Learning N: M fine-grained structured sparse neural networks from scratch. *CoRR abs/2102.04010* (2021). URL <https://arxiv.org/abs/2102.04010>. 2102.04010.
- [57] Fahim, F. *et al.* hls4ml: An open-source codesign workflow to empower scientific low-power machine learning devices. *CoRR abs/2103.05579* (2021). URL <https://arxiv.org/abs/2103.05579>. 2103.05579.
- [58] Alessandro, Franco, G., nickfraser, Umuroglu, Y. & vfdev. Xilinx/brevitas: Release version 0.2.1 (2021). URL <https://doi.org/10.5281/zenodo.4507794>.
- [59] Paszke, A. *et al.* Pytorch: An imperative style, high-performance deep learning library. In Wallach, H. M., Larochelle, A. P., Beygelzimer, A. P., d’Alché Buc, A. P. & Fox, A. P. B. (eds.) *Proceedings of the 33rd International Conference on Neural Information Processing Systems* (Curran Associates Inc., Red Hook, NY, USA, 2019).
- [60] Umuroglu, Y. *et al.* FINN: A framework for fast, scalable binarized neural network inference. In *Proceedings of the 2017 ACM/SIGDA International Symposium on Field-Programmable Gate Arrays* (ACM Press, 2017). 1612.07119.

- [61] Blott, M. *et al.* FINN-R: An end-to-end deep-learning framework for fast exploration of quantized neural networks. *ACM Trans. Reconfigurable Technol. Syst.* **11** (2018). 1809.04570.
- [62] Bengio, Y., Léonard, N. & Courville, A. C. Estimating or propagating gradients through stochastic neurons for conditional computation. *CoRR* **abs/1308.3432** (2013). URL <http://arxiv.org/abs/1308.3432>. 1308.3432.
- [63] Baskin, C. *et al.* UNIQ. *ACM Transactions on Computer Systems* **37**, 1–15 (2019). URL <https://doi.org/10.1145%2F3444943>.
- [64] Aarrestad, T. *et al.* Fast convolutional neural networks on fpgas with hls4ml. *Machine Learning: Science and Technology* **2**, 045015 (2021). URL <https://dx.doi.org/10.1088/2632-2153/ac0ea1>.
- [65] Sun, C., Nakajima, T., Mitsumori, Y., Horii, Y. & Tomoto, M. Fast muon tracking with machine learning implemented in fpga. *Nuclear Instruments and Methods in Physics Research Section A: Accelerators, Spectrometers, Detectors and Associated Equipment* **1045**, 167546 (2023). URL <http://dx.doi.org/10.1016/j.nima.2022.167546>.
- [66] Umuroglu, Y., Akhauri, Y., Fraser, N. J. & Blott, M. Logicnets: Co-designed neural networks and circuits for extreme-throughput applications. *2020 30th International Conference on Field-Programmable Logic and Applications (FPL)* 291–297 (2020). URL <https://doi.org/10.1109/FPL50879.2020.00055>.
- [67] Tsoi, H. F., Loncar, V., Dasu, S. & Harris, P. Symbolnet: Neural symbolic regression with adaptive dynamic pruning (2024). 2401.09949.
- [68] Pierini, M., Duarte, J. M., Tran, N. & Freytsis, M. Hls4ml lhc jet dataset (150 particles) (2020). URL <https://doi.org/10.5281/zenodo.3602260>.
- [69] Netzer, Y. *et al.* Reading digits in natural images with unsupervised feature learning. *NIPS Workshop on Deep Learning and Unsupervised Feature Learning* (2011).
- [70] LeCun, Y. *et al.* Backpropagation applied to handwritten zip code recognition. *Neural Computation* **1**, 541–551 (1989). URL <https://api.semanticscholar.org/CorpusID:41312633>.
- [71] Chellapilla, K., Puri, S. & Simard, P. High Performance Convolutional Neural Networks for Document Processing. In Lorette, G. (ed.) *Tenth International Workshop on Frontiers in Handwriting Recognition*. Université de Rennes 1 (Suvisoft, La Baule (France), 2006). URL <https://inria.hal.science/inria-00112631>. [Http://www.suvisoft.com](http://www.suvisoft.com).
- [72] Tange, O. Gnu parallel 20240122 ('frederik x') (2023). URL <https://doi.org/10.5281/zenodo.10558745>. GNU Parallel is a general parallelizer to run multiple serial command line programs in parallel without changing them.